

Observed dawn and twilight pressure fluctuation in the global Martian surface and possible relationships with atmospheric tides

Chengyun Yang¹, Cong Sun¹, Zhaopeng Wu², and Tao Li¹

¹University of Science and Technology of China

²Sun Yat-sen University

December 7, 2022

Abstract

Insight and other observations of the Martian surface at different locations have recorded the diurnal variation in surface pressure (Ps) with two rapid fluctuations that occur at dawn and dusk (around LT0800 and LT2000). These short-period surface pressure perturbations at specific local times are typically observed near Martian equinox. Similar phase-locked surface pressure fluctuations over most areas of the middle and low latitudes are simulated by the Martian General Circulation Model at the Dynamic Meteorology Laboratory (LMD). This phenomenon is thus likely to be global rather than local. By reconstructing the surface pressure variation from the horizontal mass flux, the pressure fluctuations in a sol can be attributed to the diurnal variation in the horizontal wind divergence and convergence in the Martian tropical troposphere in the GCM simulations. The background diurnal variation in Ps is related to the diurnal migrating tidal wind, while the enhanced convergence due to the overlap of the 4-hour and 6-hour tides before LT0800 and LT2000 is responsible for the Ps peaks occurring at dawn and twilight. Although the amplitudes of the 4-hour and 6-hour tides are smaller than those of diurnal tides, the phases of these tides remain similar in the Martian troposphere, which suggests that the convergences and divergences due to 4 h/6 h tidal winds at different altitudes are in phase and together create a mass flux comparable to that induced by diurnal/semidiurnal components and lead to rapid pressure fluctuations.

Observed dawn and twilight pressure fluctuation in the global

Martian surface and possible relationships with atmospheric tides

Chengyun Yang^{1,2,3#}, Cong Sun^{2#}, Zhaopeng Wu^{3,4}, and Tao Li^{1,2,3*}

¹Deep Space Exploration Laboratory / School of Earth and Space Sciences, University of Science and Technology of China, Hefei, Anhui, China

² CAS Key Laboratory of Geospace Environment, School of Earth and Space Sciences, University of Science and Technology of China, Hefei, Anhui, China

³ CAS Center for Excellence in Comparative Planetology, University of Science and Technology of China, Hefei, Anhui, China

⁴ Planetary Environmental and Astrobiological Research Laboratory, School of Atmospheric Sciences, Sun Yat-sen University, Zhuhai 519082, China

Correspondence to: Tao Li (litao@ustc.edu.cn)

These authors contributed equally to this work

Abstract

Insight and other observations of the Martian surface at different locations have recorded the diurnal variation in surface pressure (P_s) with two rapid fluctuations that occur at dawn and dusk (around LT0800 and LT2000). These short-period surface pressure perturbations at specific local times are typically observed near Martian equinox. Similar phase-locked surface pressure fluctuations over most areas of the middle and low latitudes are simulated by the Martian General Circulation Model at the Dynamic Meteorology Laboratory (LMD). This phenomenon is thus likely to be global rather than local. By reconstructing the surface pressure variation from the horizontal mass flux, the pressure fluctuations in a sol can be attributed to the diurnal variation in the horizontal wind divergence and convergence in the Martian tropical troposphere in the GCM simulations. The background diurnal variation in P_s is related to the diurnal migrating tidal wind, while the enhanced convergence due to the overlap of the 4-hour and 6-hour tides before LT0800 and LT2000 is responsible for the P_s peaks occurring at dawn and twilight. Although the amplitudes of the 4-hour and 6-hour tides are smaller than those of diurnal tides, the phases of these tides remain similar in the Martian troposphere, which suggests that the convergences and divergences due to 4 h/6 h tidal winds at different altitudes are in phase and together create a mass flux comparable to that induced by diurnal/semidiurnal components and lead to rapid pressure fluctuations.

Plain Language Summary

With the help of InSitu observations of Martian landers and rovers, the near-surface

pressure fluctuations in different locations are recorded, which are present near dawn and twilight with sudden pressure peaks. In previous studies, the reason for similar pressure fluctuations was attributed to buoyancy waves driven by nearby topographic effects. Nevertheless, the phase-locked sudden pressure peaks recorded at different locations challenge this hypothesis and imply a possible relationship with atmospheric tides, which are global-scale variations caused by solar heating synchronously changing with local solar time. In this study, the pressure fluctuations recorded by different landers are attributed to the diurnal variation in the horizontal wind divergence and convergence in the Martian troposphere. The zonal wind variation with periods of 4 and 6 hours mainly contributes to the observed fluctuations, while the meridional wind and diurnal/semidiurnal winds offer a background for the diurnal pressure cycle.

Key Points

1. The phase-locked surface pressure fluctuations in the Martian tropics are observed by Insight and other missions at different locations.
2. The surface pressure fluctuations are primarily attributed to the mass flux due to the horizontal wind in the Martian troposphere.
3. The interaction of the 4-hour and 6-hour tidal winds results in phase-locked morning and evening rapid pressure fluctuations.

1 Introduction

Although Mars is a cold desert with a thin atmosphere that has an average of 0.6%

of the surface pressure (P_s) compared to Earth, energetic meteorological phenomena at different spatial and temporal scales are present on Mars. The magnitude of those activities can be even stronger than those on Earth, while relevant studies on Mars are inadequate (R.M. Haberle et al., 2017; Wu et al., 2022). Mars's unique atmospheric regime offers the opportunity to study meteorological phenomena. In-situ observation at Mars's surface provides ground truth to benefit the understanding of the atmospheric variability in large-scale weather to small-scale turbulence on Mars. With the help of the recent landers and rovers, which measure the Martian meteorological field near the Martian surface, there are many highly sensitive observations to monitor activities from seasonal changes to convective vortices as well as turbulence in the Martian planetary boundary layer (PBL) (Hess et al., 1977; Banfield et al., 2020; Spiga et al., 2021; S.D. Guzewich et al., 2021).

At the synoptic scale, the early in situ observations of the Viking missions recorded seasonal baroclinic (Tillman, 1988; Collins et al., 1996) and barotropic traveling waves at their landing points (VL1 at 22.697°N , 312.05°E , VL2 at 47.64°N , 225.71°W , respectively), which is similar to the fronts and storm system on Earth (e.g., Wilson et al., 2002). On the time scale of a sol, the Viking missions first reveal vibrant diurnal variations in P_s . The P_s increases during the nighttime and reaches its maximum at approximately LT0800 in the morning, then decreases during the daytime, reaching its minimum at approximately LT1700 in the afternoon, with a diurnal range (max - min) of surface pressure of approximately 20 Pa, which is in excess of 2.6% of the mean pressure in a sol (Hess et al., 1976a; Hess et al., 1977). The Mars Pathfinder (Golombek

85 and Matthew, 1997), with a higher sampling frequency among the 3-min default
86 measurement sessions for nominally 51 times per sol on Ares Vallis, Chryse Planitia
87 ($19^{\circ}\text{N}, 33.2^{\circ}\text{W}$), recorded a daily pressure cycle that was characterized by a significant
88 semidiurnal oscillation with two maxima near LT0800 and LT2000 during its first 30
89 sol observations (Haberle et al., 1999). With the improvement of the detection
90 capability in both sampling frequency and precision, the surface pressure observed by
91 the Curiosity mission landing in Gale Crater ($4.5^{\circ}\text{S}, 137.73^{\circ}\text{E}$) recorded a clear diurnal
92 cycle along with short-period Ps fluctuations from tens of minutes to 3 hours (S.D.
93 Guzewich et al., 2021). Notably, the strong spectral powers are conspicuous near
94 LT0800 and LT2000, especially during sols near the equinox, suggesting vibrant
95 fluctuations in the morning and evening, respectively. The initial observation from the
96 recent Insight mission, which is the first continuously operating meteorological detector
97 on the Martian surface landing on the Elysium Planitia ($4.5^{\circ}\text{N}, 135.6^{\circ}\text{E}$), which is
98 located across the equator from the Curiosity rover, also records the rapid pressure
99 fluctuations in the morning and evening after the “type C” large dust storm in MY34
100 (~ 45 sol in the Insight observation), in addition to the diurnal and semidiurnal pressure
101 variations that are mentioned by past landers and rovers (Banerdt et al., 2020; Bandfield
102 et al., 2020). In the rest of this paper, the sudden increasing surface pressure peaks near
103 LT0800 and LT2000 are denoted by the “Dawn & Twilight peaks” (DTPs/DP and TP,
104 respectively). The Ps on Earth also shows a similar pattern of diurnal and semidiurnal
105 variation but with much smoother peaks and take place at different local times (maximal
106 values are present near LT1000 and LT2200 in the low latitude observations), which

107 implies that DTPs on Mars is a unique phenomenon (Le Blance, 2011). The
108 investigation of the mechanisms that modulate the daily variation in Martian surface
109 pressure, which is distinct from its neighboring Earth, can be a unique opportunity to
110 provide a fresh understanding of the atmospheric environment in the different planets.

111 Although DTPs near LT0800 and LT2000 have been reported by both Curiosity
112 and Insight missions, the underlying mechanism has not been well established. Hourdin
113 et al. (1993) suggested that the surface pressure variations may partly be due to
114 orographic effects. Guzewich et al. (2021) suggested that the sudden surface pressure
115 fluctuations observed by Curiosity are related to buoyancy waves driven by the airflow
116 over the nearby topography at dawn and twilight. However, the in situ observations of
117 multiple landers and rovers also showed similar rapid Ps fluctuations, implying the
118 contribution of other mechanisms in addition to the effect of local topography.

119 Atmospheric thermal tides are global-scale harmonic waves induced by solar
120 heating across the planet (Gierasch & Goody, 1968; Zurek, 1976). The amplitude of
121 atmospheric thermal tides is usually large because of the low heat capacity of Martian
122 air and dominates the diurnal pressure and temperature variations in the Martian
123 atmosphere (Fan et al., 2022). Thermal tides can cause large-scale divergence and
124 convergence of the atmosphere, which play a potential role in surface pressure
125 variations (Wu et al., 2020).

126 The goal of this study is to investigate the possible mechanisms that lead to the
127 sudden increasing dawn and twilight surface pressure peaks in a daily cycle using both
128 in situ observations and GCM simulations. Section 2 introduces the datasets of in situ

observations and GCM simulations and the method used to process the data in this study. In Section 3, the phenomenon of Martian surface pressure fluctuations near LT0800 and LT2000 are described based on Martian landers and rovers observations. Section 4 discusses the possible mechanism by which global daily Ps variations are modulated. A summary of the findings of this study and a discussion of the implications are provided in Section 5.

2 Data and Method

2.1 Observations

The Insight mission, which landed at Elysium Planitia (4.5°N 135.6°E) in the northern winter, became the first continuously operating meteorological station on the Martian surface (Banerdt et al., 2020; Spiga et al., 2018). The pressure data are derived from the high-precision pressure sensor (PS), which is a part of the Auxiliary Payload Sensor Subsystem (APSS) (Banfield et al., 2019). With sensors onboard the Insight lander that worked in continuous mode for nearly 2 Martian years, InSight provided one of the most valuable records to study the near-surface atmosphere on Mars.

The pressure records samples at frequencies ranging from 2 to 10 Hz during the Insight mission, covering 88% of the first 170 sols in MY35 (Viúdez-Moreiras et al., 2020; Chatain et al., 2021).

Data from other Mars landers and rovers, including Vikings (VLs), Mars Pathfinder (MPF), Mars Science Laboratory (MSL), and Perseverance, are also adopted in this

study. The Viking Meteorology Instrument System (VMIS) onboard VL1 and VL2 consisted of sensors to measure pressure, temperature, and wind near the Martian surface, which landed on Mars in 1976 (Hess et al., 1976a; Hess et al., 1976b; Hess et al., 1977). The Viking landers worked in modules of 9 min, 20 min or 39 min to measure these meteorological variables at different sampling rates, spaced from 1.5 h apart in a sol. VL1 landed at 22.4°N and worked for 2245 sols, while VL2 landed at 47.9°N and operated for 1281 sols (Chamberlain et al., 1976). The Atmosphere Structure Instrument/Meteorology Package (ASI/MET) experiment on board the MPF lander started its mission in July 1997 near the "Ares Vallis" (33.52°W, 19.30°N), which also has the ability to measure surface pressure at high quality (Golombek, 1997). A detailed introduction of the MPF observation mode can be found in the reference (Golombek, 1997; Schofield et al., 1997; Savijärvi et al., 2004). The Mars Science Laboratory (MSL) onboard the Curiosity rover landed in Gale crater (137.42°E, 4.6°S) in August 2012 and measured air pressure at a height of 1 m on the rover deck (Gómez-Elvira et al., 2012). The MSL pressure sensor sample was 5 min long per hour at 1 Hz throughout the mission with an interspersed full hour sample period for over 3580 sols. The Mars Environmental Dynamics Analyzer (MEDA) onboard the Perseverance rover consists of a pressure sensor, which measures the surface pressure with a sampling rate of 1 Hz in every observation group, while every group has a gap of at least an hour or even more (Rodriguez-Manfredi et al., 2021; Jackson, 2022).

The observation data mentioned above can be found on the Planetary Atmospheres Node (ATM) of the Planetary Data System (PDS), <https://pds->

atmospheres.nmsu.edu/#Mars.

2.2 GCM Simulations

A series of Martian general circulation models (GCMs) at the Dynamic Meteorology Laboratory (LMD) (Forget et al., 1999) were conducted for comparison with in situ observations. The Martian LMD model consists of a dynamical core, which integrates hydrodynamic equations with a finite difference method, and a rigorous physical core, which takes into account radiative transfer (Forget et al., 1999), the dust cycle (Madeleine et al., 2011), the water cycle (Madeleine et al., 2012; Montmessin et al., 2004; Navarro, Madeleine et al., 2014), PBL transferring (Colaïtis et al., 2013) and other physical processes (e.g., Forget et al., 1999; Forget et al., 2011). In our study, the simulations are conducted with a resolution of $5.625 \times 3.75^\circ$ in the horizontal direction and 29 levels in the vertical direction from the ground to 100 km. To correspond with the dust scenario during the Insight mission, the MY34 and MY35 reconstructed dust maps are used as initial model files (a detailed introduction of the dust maps can be found in Montabone et al., 2020). The output data in a sol have been set to 48 times per sol to capture the short-period atmospheric fluctuations.

2.3 Data Processing Methods

To investigate the daily atmospheric variation related to the Ps fluctuations and

reveal the characteristics of the Ps variation with different periods, the daily mean value is first excluded from the data. Then, the harmonic fit is utilized to subtract the short period variations from the diurnal cycle (e.g., R. Haberle et al., 2014; S. Guzewich et al., n.d.; S. D. Guzewich et al., 2021). The periodicity characteristics of the observed pressure data are evaluated by the Lomb-Scargle (LS) Periodogram (Lomb, 1981; Scargle et al., 1982), which is designed to detect the periodicity in both evenly and unevenly sampled time series. In this study, the LS Periodogram is conducted with an uncertainty of 10 mPa (Lange et al., 2022).

Martian thermal tides are traveling waves in the atmosphere induced by the solar heating of gases and aerosols, which are typically water ice and dust on Mars (Guzewich, Tiogo, et al., 2013; Hinson and Wilson, 2004; Kleinböhl et al., 2013; Wilson and Guzewich, 2014; Wu et al., 2017). The migrating tide is phase-locked in local solar time (Zurek et al., 1979, 1981). The amplitude and phase are two basic parameters used to identify the characteristics of thermal tides (Chapman and Lindzen, 1970; Forbes, 1995; She et al., 2016). As propagating waves in the atmosphere in both longitudinal and vertical directions, thermal tides can be characterized as a series of harmonic functions (Chapman and Lindzen, 1970; Forbes, 1995). The certain tidal component from the original meteorological field can be expressed as follows, in line with previous studies (e.g., Banfield et al., 2000; Wu et al., 2015, 2017):

$$P(\lambda, \phi, p, t) = \sum_{\sigma, s} (C_{\sigma, s}(\phi, p) \cos(s\lambda + \sigma t) + S_{\sigma, s}(\phi, p) \sin(s\lambda + \sigma t)) \quad (1)$$

where λ , ϕ and p are the longitude, latitude and pressure level, respectively; t is the universal time; s and σ are the wavenumbers in longitude and time space; and C

and S are the amplitudes of the harmonic functions. The amplitude (A) and phase (θ) of each mode can be obtained by:

$$A_{\sigma,s}(\varphi, p) = \sqrt{C_{\sigma,s}(\varphi, p)^2 + S_{\sigma,s}(\varphi, p)^2} \quad (2)$$

$$\theta_{\sigma,s}(\varphi, p) = \tan^{-1} \left(\frac{C_{\sigma,s}(\varphi, p)}{S_{\sigma,s}(\varphi, p)} \right) \quad (3)$$

According to the hydrostatic assumption, the surface pressure is determined by the mass accumulation of the whole atmosphere (Andrews et al., 1987). The surface pressure can be reconstructed using the horizontal wind from a certain vertical range as:

$$P_{\text{recon}} = \int_t \int_{hs}^{he} -\nabla \cdot \vec{w} \cdot \rho \cdot D dz dt \quad (4)$$

where t is time; z is vertical height; hs and he indicate the height range used to calculate the mass flux; \vec{w} is the horizontal wind; ρ is the density; D is calculated as $D = \frac{g}{aire}$, while $aire$ is the area of the longitude-latitude grid, and g is the gravitational acceleration.

3 Results

Figure 1 shows the surface pressure observed by Insight (blue line) in five continuous sols near the equinox ($L_s = \sim 0^\circ$). The surface pressure observation from the Insight mission shows a significant diurnal cycle with a maximum of ~ 745 Pa near LT0800 in the morning and a minimum of ~ 705 Pa near LT1700. The amplitude of the P_s diurnal variation is approximately 40 Pa in a sol, 5.5% of the daily mean pressure, which is much larger than that on Earth (approximately 0.8%). In addition to the diurnal variation, which is characterized by the P_s decreasing in the daytime and increasing in

the nighttime, there are two sudden increases in the pressure near LT0800 and LT2000. The timescale of the P_s fluctuation near LT0800 and LT2000 is much shorter than the diurnal or semidiurnal cycle. The pressure peak in the morning is usually the daily maximum (larger than in the evening), with a sudden pressure increase of approximately 15 Pa from LT0600 to LT0800, which is approximately 2% of the daily mean pressure. From LT0800 to LT1000, the pressure drops down to a similar value at LT0600. The rapid increase and decrease in P_s in the evening overlapped with the increasing P_s due to the diurnal cycle. The pressure begins to increase from ~LT1630 with the lowest P_s in a sol and increases to its maximal of 40 Pa near LT2000, then drops down and reaches the minimal value near LT2200. In the rest of this paper, the sudden increasing surface pressure peaks near LT0800 and LT2000 are denoted by the “Dawn & Twilight peaks” (DTPs/DP and TP, respectively).

The dawn pressure peaks are identified when a rapid pressure increase occurs with an amplitude over 1.5% of the daily mean pressure from LT0600 to LT0800, while the twilight pressure peaks are identified when the pressure rapidly increases with an amplitude over 1% of the daily mean pressure. **Figure 2** shows the occurrence of the surface pressure observations that dawn and twilight pressure fluctuations are present after the landing of the Insight mission for over 1 Martian year. The labels of “DTPs”, “NDTPs” and “MD” represent the sols that the DTPs are present, not present or missing data to determine the DTPs, respectively. During the observation of the InSight mission for one Martian year, the DTPs prefer to occur near the equinox and can last for over 100 sols, so it can be regarded as a general phenomenon near the

Martian equator.

In addition to the Insight mission, which is located near the Martian equator, the diurnal variation in the surface pressure is also recorded by other landers and rovers at different locations (**Figure 3**). The missions at low latitudes, such as the Insight and Curiosity missions, show strong diurnal and semidiurnal variations associated with significant DTPs, while the similar DTPs recorded at higher latitudes are weaker than those observed at low latitudes (Guzewich et al., 2021; Banfield et al., 2020). The observations in the middle latitudes, such as the VLs, MPF, and perseverance missions, also suggested similar phase-locked DTPs with weaker amplitudes compared to the observations near the equator, such as the Insight and Curiosity missions. The observed Ps fluctuations are well fitted with the properties of buoyancy waves forced by airflow over local topography (Guzewich et al., 2021). However, as the landers and rovers in either low latitudes or middle latitudes with different topographic conditions show Ps variation with DTPs, the DTPs should not be mainly attributed to the local topography. As presented in **Figure 1**, the diurnal variation in the surface pressure in the LMD simulations (red line) around the Insight lander agrees well with that in the Insight observations, although the relative amplitude of the surface pressure diurnal cycle is larger in the simulations. The surface pressure in the LMD simulation reaches its maximum in the early morning at approximately 760 Pa, while in the afternoon near LT1700, the LMD Ps decreases to a minimum of ~700 Pa. The LMD simulation of surface pressure also presents a significant sudden pressure fluctuation in the morning and evening in addition to the diurnal or semidiurnal cycles.

As shown in [Figure 4](#), the period analyses are conducted by the Lomb Scargle periodograms for both the observations and LMD simulations. The Insight Ps (blue line) suggests the dominance of the diurnal cycle in the Ps variation with 60% of the total variation power. The semidiurnal component, with 25% of the total variation power, is the second largest component. The 8 h component, however, is quite weak in the LS periodogram in both observations and LMD simulations. The variation with periods of 6 hours and 4 hours are attributed to approximately 8% and 4% of the total Ps daily variation, respectively. The residual power from these 4 components is less than 3%, demonstrating that the daily surface pressure variation is basically controlled by 24-hour, 12-hour, 6-hour and 4-hour variations. The LS periodogram of the LMD simulations suggests a similar contribution of the variation with these four periods in the daily Ps variations ([Figure 4](#), red line). The diurnal component of the LMD simulation is larger than that of the Insight observations, which reaches 78% of the total variation power. In contrast, other components are smaller than those in the observations. The residual variation power in the LMD simulation is also less than 3%. Since the LMD simulation is consistent with the Insight observations, the LMD simulation is adopted to investigate the possible formation mechanism of the Ps daily variation and the DTPs.

As mentioned above, similar DTPs were observed at different latitudes by rovers and landers, while the LMD model simulated LMD simulations rapid Ps perturbations around dawn and twilight in the mid- and low-latitudes on Mars. It is thus implied that the potential mechanisms in addition to the local topographic effect can play an

important role in Ps daily fluctuations.

4 Discussions

As the surface pressure is mainly contributed by the hydrostatic pressure caused by the total air mass above, the Ps variation can be estimated by the variation in the mass flux in the atmospheric column induced by horizontal wind convergence or divergence (Andrews et al., 1987). To investigate the possible mechanism by which the daily variation in the atmosphere can influence the surface pressure variation, Ps is first diagnosed by reconstructing from the mass flux due to horizontal wind divergence and convergence in LMD simulations, as shown in equation 4. The reconstructed Ps (green inverted triangle in [Figure 6a](#)) using the horizontal wind (with the daily mean eliminated) at the vertical range of 0-100 km (surface to the top of LMD) well represent both the diurnal variation and semidiurnal surface pressure (red line), while there are obvious DTPs characterized by a sudden increase of 16 Pa from LT0600 to LT0800 in the morning and a sudden increase of 8 Pa from the afternoon to LT2100. The reconstruction from the 0-40 km wind (purple line) is nearly the same as that from the 0-100 km wind, which suggests that the variation in the surface pressure is mainly controlled by the wind convergence in the Martian troposphere. The rapid increases and drops in Ps are also obvious at LT0800 and LT2000 in the reconstructed Ps variation from the surface to 20 km, suggesting that the mass flux in the lower troposphere plays a dominant role in modulating the DTPs.

The DTPs recorded by different missions usually appear at approximately the same local time. As migrating thermal tides can induce local time-dependent horizontal wind convergence and divergence at different locations, they may play an important role in these phase-locked surface pressure fluctuations observed by multiple landers and rovers in different locations.

As shown in **Figure 6b**, the surface pressure reconstruction from the meridional term of the migrating tidal wind with periods of 4 hours (4 h), 6 hours (6 h), 12 hours and 24 hours (yellow line) shows a diurnal cycle with a peak of ~ 14 Pa near LT0800. The Ps reconstructed by meridional tidal wind shows a smooth variation of Ps, which implies that the DTPs should not be attributed to the meridional tidal wind. The reconstructed Ps by the diurnal and semidiurnal tidal zonal wind show a diurnal Ps variation with the maximum during the midnight and minimum during the midday, which is approximately out of phase with the Ps diurnal variation due to the meridional tidal wind.

The Ps variation due to 4 h and 6-h migrating tidal zonal winds (red line) shows a rapid variation with amplitudes of approximately 15-20 Pa near LT0800 and LT2000 (**Figure 6c**). Associated with the smooth Ps peaks due to the semidiurnal tidal zonal wind, the 4-h and 6-h tidal winds together contribute to the Ps peaks at approximately LT0800 and LT2000 in the reconstructed Ps.

As shown in **Figure 7b**, the vertical wavelengths of both the 4 h component and the 6 h component are very long, with almost the same tidal phase in the vertical range of the troposphere. The phase of the 4 h component is approximately 2 LT (around π),

while the phase of the 6 h tidal component is approximately $4.5 - 5.2$ LT ($3/2 \pi$ to $7/4 \pi$), which means that the zonal convergence between the peaks (maximum of the eastward tidal wind) and troughs (maximum of the westward tidal wind) due to the 4 h tide occurs from LT0200 to LT0400 and occurs every 4 hours thereafter, while the convergence due to the 6 h tidal zonal wind occurs approximately between LT0500 and LT 0800 and occurs every 6 hours thereafter. The convergence due to the two tidal zonal winds overlaps with each other before LT0800 and meets each other again from LT1800 and LT2000, which leads to positive mass flux increases ~ 2 hours before the pressure peaks (LT0600-0800 and LT 1800-2000, respectively), which in turn causes the LT0800 and LT2000 pressure peaks at middle and low latitudes on a global scale (**Figure 6d**). Although the amplitude of the migrating diurnal tide (DW1, **Figure 7a**) is larger than that of either 4 h or 6 h tide, the DW1 horizontal wind convergences in the lower and upper troposphere reverse with each other due to the relatively short vertical wavelength and then leads to limited contribution to the total mass flux and Ps variation. The 4-h and 6-h zonal tidal winds, which become in phase with each other with a 12-hour interval, contribute primarily to the DTPs present at LT0800 and LT2000. As shown in **Figure 6d**, the 6 h zonal tidal wind provides a slightly greater contribution to the DPs, while in the TPs, the 4 h and 6 h zonal tidal winds contribute nearly the same in the pressure peaks. The 4 h zonal tidal wind tends to induce a sharper pressure fluctuation, which manifests as a rapid pressure increase both ~ 2 h before DPs and TPs. The reconstruction of all of these tidal components (black line) agrees with the reconstruction from the 0-40 km horizontal wind, although the fluctuations in other

local times (especially from noon to LT1600) appear to be more vibrant than those in both the observations and simulations.

As shown in **Figure 8**, the negative wind divergence, indicating the increased incoming mass flux, is present from LT0600 to LT0800 in the upper and middle troposphere and near the surface (**Figure 8a, 8b and 8c**, the left column of **Figure 8**), which corresponds to the rapid Ps increase at LT0800. The mass-weighted wind divergence in the morning (LT0600 to LT0800) is negative in the upper troposphere (**Figure 8a**) but much weaker than that in the middle troposphere (**Figure 8b**) and near the surface (**Figure 8c**), which is approximately $-1 \sim -2 \times 10^{-8} \text{ kg m}^{-3} \text{ s}^{-1}$. From LT1800 to LT2000, before the twilight pressure peak, the amplitudes of the mass-weighted wind divergence are $-0.4 \times 10^{-8} \text{ kg m}^{-3} \text{ s}^{-1}$ and $-0.6 \times 10^{-8} \text{ kg m}^{-3} \text{ s}^{-1}$ near 20 km and 40 km, respectively, while the convergence near the surface is stronger with a mass-weighted divergence of approximately $-5 \times 10^{-8} \text{ kg m}^{-3} \text{ s}^{-1}$. It is suggested that the mass convergence near the surface and in the upper troposphere contributes primarily to the twilight Ps peaks at LT2000. The right column (**Figure 8d, 8e and 8f**) shows the 4 h and 6 h migrating tidal horizontal winds and their mass-weighted divergence, whose phases are nearly unchanged in the troposphere (**Figure 7b**). The mass-weighted wind divergences induced by 4 h and 6 h zonal tidal winds before the morning pressure peaks are approximately $-0.2 \times 10^{-8} \text{ kg m}^{-3} \text{ s}^{-1}$ at 40 km, $-0.4 \times 10^{-8} \text{ kg m}^{-3} \text{ s}^{-1}$ at 20 km and $-2 \times 10^{-8} \text{ kg m}^{-3} \text{ s}^{-1}$ in the near surface, 20 km and upper troposphere, respectively, which agree well with the divergence caused by the horizontal wind. On the other hand,

before the evening pressure peaks, the mass-weighted wind divergences are $-2.5 \times 10^{-8} kg m^{-3} s^{-1}$ at the surface, $-0.5 \times 10^{-8} kg m^{-3} s^{-1}$ at 20 km and $-0.1 \times 10^{-8} kg m^{-3} s^{-1}$ at 40 km. These negative wind divergences induced by the zonal tidal winds at different levels in the troposphere coincide well with the divergence in the previous ~ 2 h of the DTPs, as shown in the left column. Thus, the convergence due to the 4-h and 6-h zonal tidal winds plays a dominant role in creating DTPs in the global tropics on Mars.

The similar tidal decomposition conducted on other sols with the occurrence of DTPs suggested that the 4 h and 6 h tidal wind components also play a dominant role in creating the DTPs during other sols near equinox, as shown in [Figure S1](#).

5 Summary

The sudden increased surface pressure, characterized by the pressure peaks present at approximately LT0800 in the morning and LT2000 in the evening, which implies a phase-locked pattern on a global scale, has been recorded by different in situ Martian landers and rovers at various locations. The LMD simulations reproduce the surface pressure fluctuations at nearly the same local time. With the help of the periodicity spectrum analysis, the daily surface pressure variation from both the observations and simulations is primarily controlled by the diurnal, semidiurnal, 6 h and 4 h variations.

The reconstructed surface pressure by the horizontal wind suggested that the mass flux due to the horizontal wind in the troposphere dominate the diurnal variation in the

surface pressure. The tidal meridional wind associated with the DW1/SW2 tidal zonal wind contributes primarily to the diurnal cycle of the surface pressure. On the other hand, the combined influence of the 4-h and 6-h zonal tidal winds contributes primarily to the DTPs near LT0800 and LT2000. The vertical wavelengths of the 4 h and 6 h zonal tidal wind components are very large, with almost constant phases in the Martian troposphere. As a result, the wind divergence in the entire mid- and low-latitude troposphere becomes negative before LT0800 and LT2000, respectively, which in turn leads to a rapid increase in surface pressure. The peaks of the 4 h and 6 h tides overlap with each other twice a day, causing two surface pressure peaks 12 hours apart from each other.

With the help of more overlapping observations of multiple Martian landers and satellites, investigations finding evidence of the possible energy source inducing high-order tidal components are becoming feasible. Future works should be reserved to explore the potential mechanisms generating the 4 h/6 h tides in the atmosphere using recent satellites covering multiple local times and simultaneous observed meteorological stations on Martian landers and rovers.

Acknowledgment

This work was supported by the National Natural Science Foundation of China grants (42275133, 42130203, 41874180, 41974175, 41831071); the B-type Strategic Priority Program of the Chinese Academy of Sciences, grant no. XDB41000000; the

preresearch project on Civil Aerospace Technologies no. D020105 funded by China's National Space Administration; and the Open Research Project of Large Research Infrastructures of CAS—"Study on the interaction between low/mid-latitude atmosphere and ionosphere based on the Chinese Meridian Project". Chengyun Yang and Cong Sun contributed equally to this work.

Data Availability Statement

The observation data of the Insight mission are available at https://atmos.nmsu.edu/data_and_services/atmospheres_data/INSIGHT/insight.html.

Observation data from other missions can be found on the Planetary Data System at <https://pds-geosciences.wustl.edu/missions/mep/index.htm>. The model outputs used in this work are available on the Open Science Framework at https://osf.io/gqdsc/?view_only=34a462b55e6c40a683c8011162ae50e5.

Figure Captions

Figure 1. The surface pressure measured by InSight Rover and simulated from LMD near the InSight location. The red line indicates the LMD results, and the blue line indicates the observation from InSight.

Figure 2. The occurrence of the surface pressure observations show that dawn and twilight pressure (DTPs) are present after the landing of the InSight mission on the Martian surface and last for over 700 sols (from the end of MY34 to MY35 over a Martian year). The MD labels the sols that the pressure data are insufficient to judge whether DTPs are present or not.

Figure 3. In situ observations of surface pressure in a sol by multilanders and rovers at different locations with daily mean pressure removed.

Figure 4. Lomb-Scargle periodograms for the surface pressure observed by InSight and simulated by LMD are shown in Figure 1. The periods of 24, 12, 6 and 4 hours are highlighted by the dotted vertical lines.

Figure 5. The LMD simulated zonal mean surface pressure with the same local time near InSight sol 125 at different latitudes with the daily mean value removed.

Figure 6. (a) Daily variation of the P_s (red line) and the P_s reconstructed by the daily horizontal winds variations with daily mean removed from surface to 100 km (green triangles), from surface to 40 km (the pinkish red line) and from surface to 20 km (blue plus signs); (b) the daily variation of the P_s reconstructed by the daily horizontal winds variations (the pinkish red line, as in (a)), the migrating tidal winds (both zonal and meridional winds, black line), the migrating tidal meridional winds (black line) and

diurnal and semidiurnal migrating tidal zonal winds (gramineous line) from surface to 40 km; (c) Reconstructed Ps by the 4- and 6-hour zonal tidal winds (red line and plus sign), the semidiurnal tidal wind (green line); (d) Reconstructed Ps the 4-hour migrating tidal zonal wind (light green dashed line) and 6-hour migrating tidal zonal wind (the green dashed line). The red line is the reconstructed surface pressure from the sum of the 4 h and 6 h tidal zonal winds, which is the same as the red line in (c).

Figure 7. Vertical profiles of the (a) amplitude and (b) phase of the 4 h, 6 h, 12 h and 24 h tidal zonal winds. The blue, pinkish red, green and black lines represent the tidal components at 4 h, 6 h, 12 h and 24 h, respectively. The 4 h, 6 h and 12 h zonal tidal wind amplitudes use the lower axes in subplot (a), while the DW1 wind amplitude uses the upper axes.

Figure 8. The daily variation in the horizontal wind (vectors) and its divergence (weighted by atmospheric density, shading) at (a) 40 km, (c) 20 km and (e) near the surface; (b), (d) and (f) are the same as (a), (c) and (e) but for the density-weighted 4- and 6-hour horizontal tidal wind divergence.

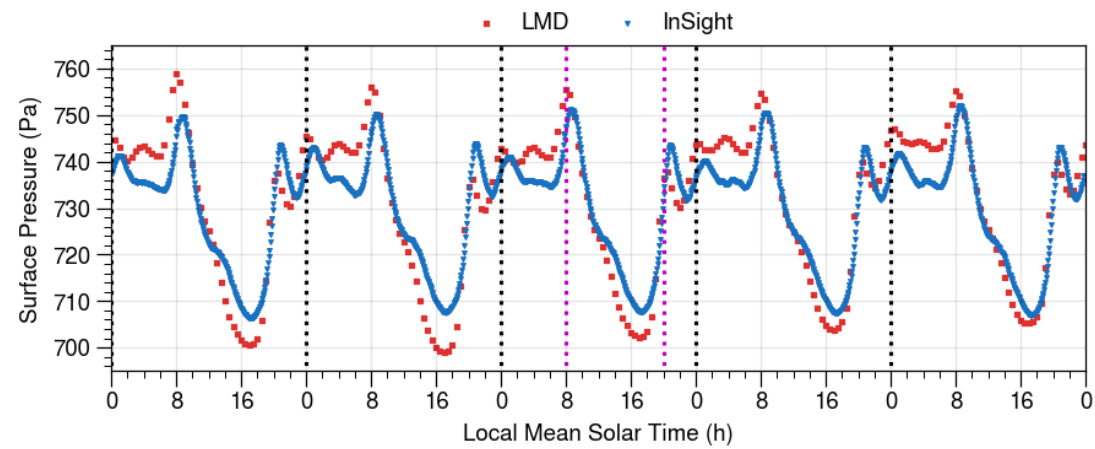


Figure 1. The surface pressure measured by InSight Rover and simulated from LMD near the InSight location. The red line indicates the LMD results, and the blue line indicates the observation from InSight.

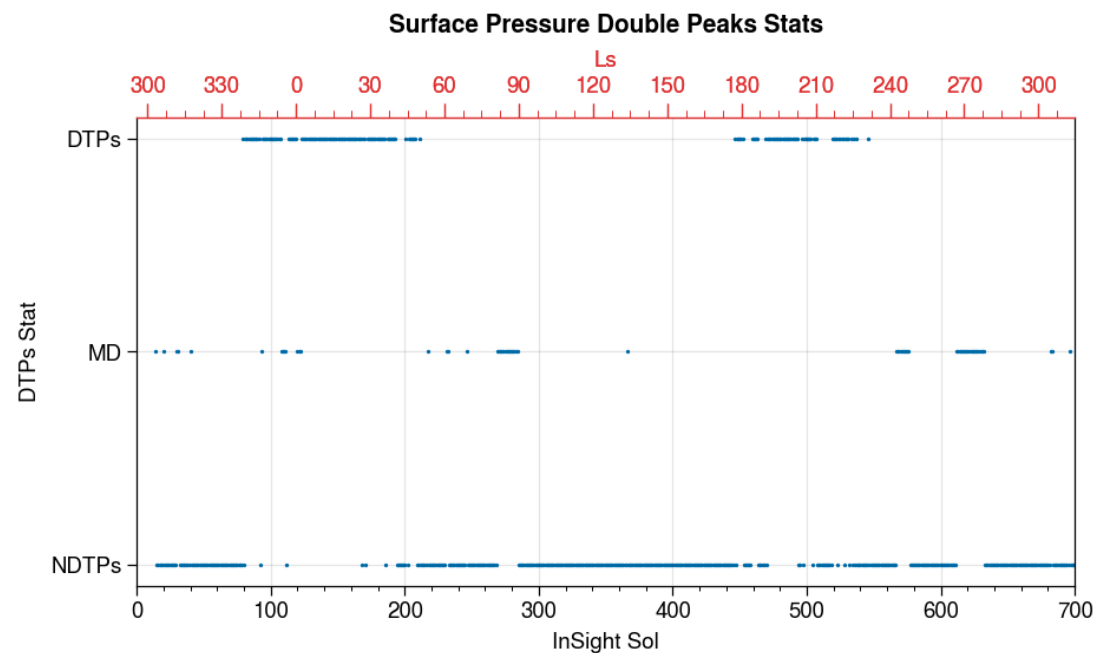


Figure 2. The occurrence of the surface pressure observations show that dawn and twilight pressure (DTPs) are present after the landing of the InSight mission on the Martian surface and last for over 700 sols (from the end of MY34 to MY35 over a

Martian year). The MD labels the sols that the pressure data are insufficient to judge whether DTPs are present or not.

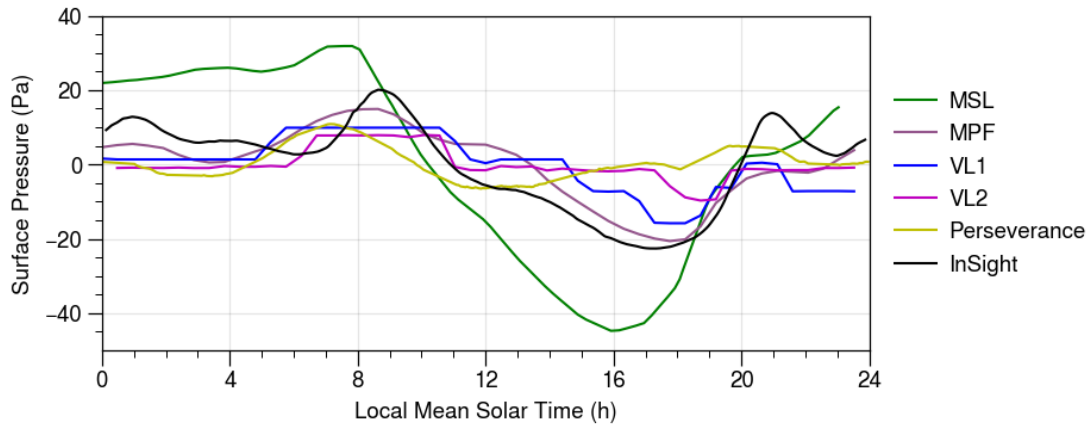


Figure 3. In situ observations of surface pressure in a sol by multilanders and rovers at different locations with daily mean pressure removed.

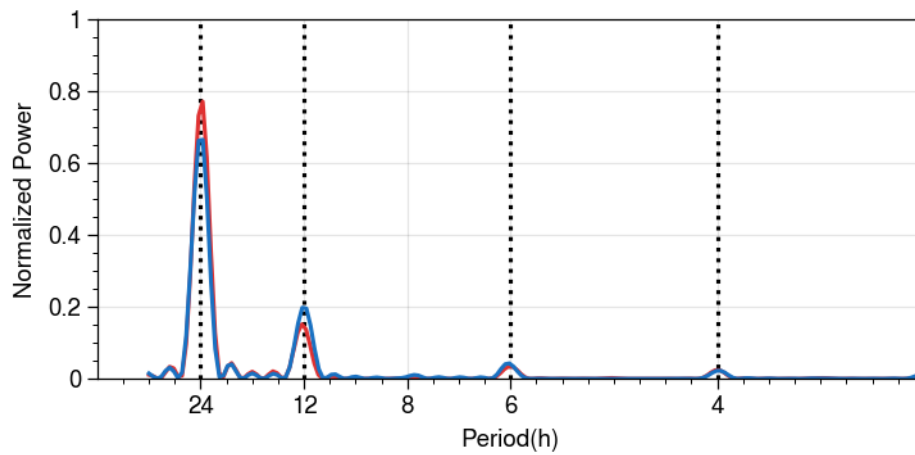
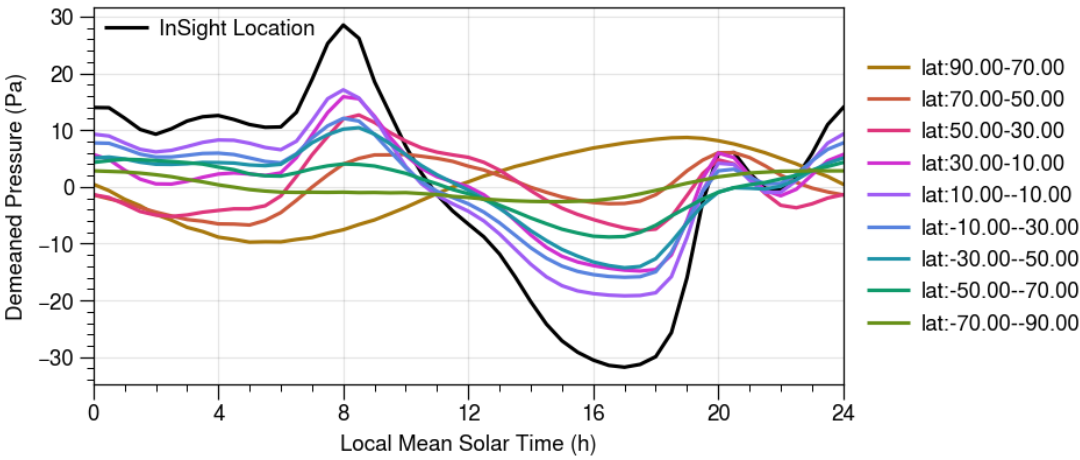


Figure 4. Lomb-Scargle periodograms for the surface pressure observed by InSight and simulated by LMD are shown in Figure 1. The periods of 24, 12, 6 and 4 hours are highlighted by the dotted vertical lines.

504



505

506 **Figure 5.** The LMD simulated zonal mean surface pressure with the same local time
507 near Insight sol 125 at different latitudes with the daily mean value removed.

508

509

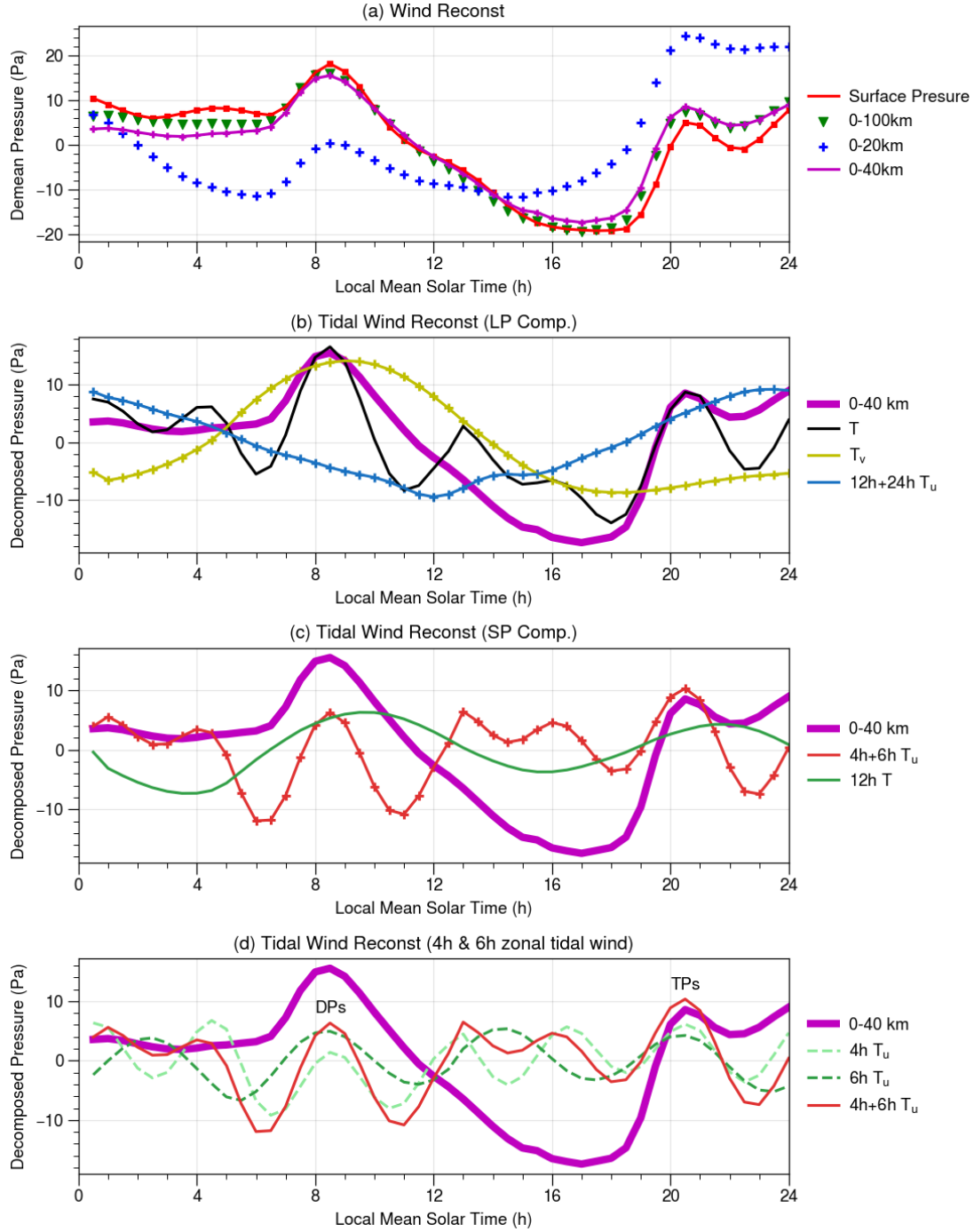


Figure 6. (a) Daily variation of the P_s (red line) and the P_s reconstructed by the daily horizontal winds variations with daily mean removed from surface to 100 km (green triangles), from surface to 40 km (the pinkish red line) and from surface to 20 km (blue plus signs); (b) the daily variation of the P_s reconstructed by the daily horizontal winds variations (the pinkish red line, as in (a)), the migrating tidal winds (both zonal and

meridional winds, black line), the migrating tidal meridional winds (black line) and diurnal and semidiurnal migrating tidal zonal winds (gramineous line) from surface to 40 km; (c) Reconstructed Ps by the 4- and 6-hour zonal tidal winds (red line and plus sign), the semidiurnal tidal wind (green line); (d) Reconstructed Ps the 4-hour migrating tidal zonal wind (light green dashed line) and 6-hour migrating tidal zonal wind (the green dashed line). The red line is the reconstructed surface pressure from the sum of the 4 h and 6 h tidal zonal winds, which is the same as the red line in (c).

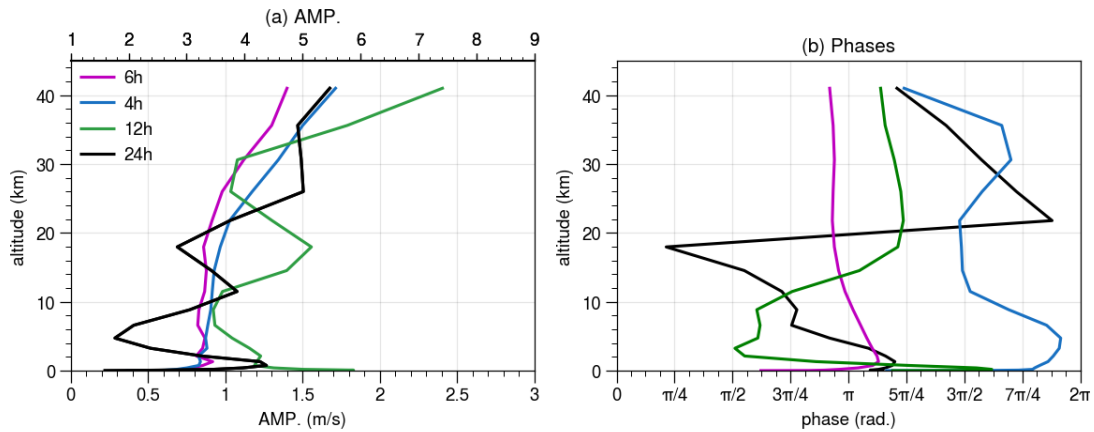


Figure 7. Vertical profiles of the (a) amplitude and (b) phase of the 4 h, 6 h, 12 h and 24 h tidal zonal winds. The blue, pinkish red, green and black lines represent the tidal components at 4 h, 6 h, 12 h and 24 h, respectively. The 4 h, 6 h and 12 h zonal tidal wind amplitudes use the lower axes in subplot (a), while the DW1 wind amplitude uses the upper axes.

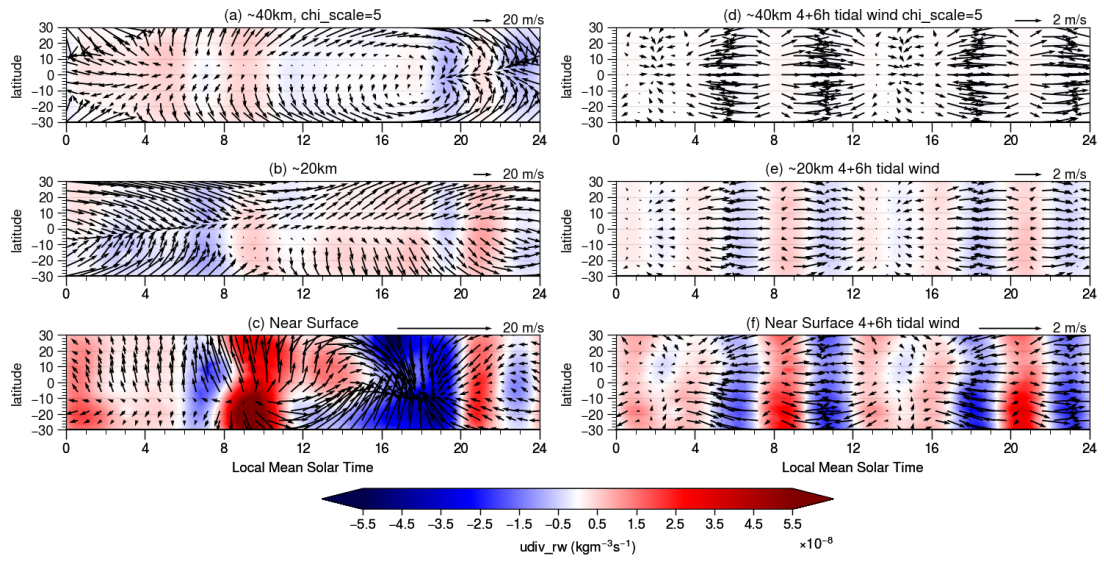


Figure 8. The daily variation in the horizontal wind (vectors) and its divergence (weighted by atmospheric density, shading) at (a) 40 km, (c) 20 km and (e) near the surface; (b), (d) and (f) are the same as (a), (c) and (e) but for the density-weighted 4- and 6-hour horizontal tidal wind divergence.

References

Banerdt, W. B., Smrekar, S. E., Banfield, D., Giardini, D., Golombek, M., Johnson, C. L., ... others (2020). Initial results from the insight mission on mars. *Nature Geoscience*, 13(3), 183–189.

Banfield, D., Rodriguez-Manfredi, J., Russell, C., Rowe, K., Leneman, D., Lai, H., ... others (2019). Insight auxiliary payload sensor suite (apss). *Space Science Reviews*, 215(1), 1–33.

Banfield, D., Spiga, A., Newman, C., Forget, F., Lemmon, M., Lorenz, R., ... others (2020). The atmosphere of mars as observed by insight. *Nature Geoscience*, 13(3), 190–198.

Chamberlain, T. E., Cole, H. L., Dutton, R. G., Greene, G. C., & Tillman, J. E. (1976). Atmospheric measurements on Mars: The Viking meteorology experiment. *Bulletin of the American Meteorological Society*, 57(9), 1094-1105.

Chatain, A., Spiga, A., Banfield, D., Forget, F., & Murdoch, N. (2021). Seasonal variability of the daytime and nighttime atmospheric turbulence experienced by InSight on Mars. *Geophysical Research Letters*, 48(22), e2021GL095453.

Collins, M., Lewis, S., Read, P., & Hourdin, F. (1996). Baroclinic wave transitions in the martian atmosphere. *Icarus*, 120(2), 344–357.

Colaïtis, A., Spiga, A., Hourdin, F., Rio, C., Forget, F., & Millour, E. (2013). A thermal plume model for the Martian convective boundary layer. *Journal of Geophysical Research: Planets*, 118(7), 1468-1487.

Fan, S., Guerlet, S., Forget, F., Bierjon, A., Millour, E., Ignatiev, N., ... & Korablev,

572 O. (2022). Thermal Tides in the Martian Atmosphere near Northern Summer Solstice
573 Observed by ACS/TIRVIM onboard TGO. *Geophysical Research Letters*, 49(7),
574 e2021GL097130.

575 Forbes, J. M. (1995). Tidal and planetary waves. *The Upper Mesosphere and Lower*
576 *Thermosphere: A Review of Experiment and Theory*, Geophys. Monogr. Ser, 87, 67-87.

577 Forget, F., Hourdin, F., Fournier, R., Hourdin, C., Talagrand, O., Collins, M., ...
578 Huot, J.-P. (1999). Improved general circulation models of the martian atmosphere
579 from the surface to above 80 km. *Journal of Geophysical Research: Planets*, 104(E10),
580 24155–24175.

581 Forget, F., Millour, E., Madeleine, J. B., Colaitis, A., Spiga, A., Montabone, L., ...
582 & Mulholland, D. (2011). Back to the basics: Improving the prediction of temperature,
583 pressure and winds in the LMD general circulation model.

584 Gierasch, P., & Goody, R. (1968). A study of the thermal and dynamical structure
585 of the Martian lower atmosphere. *Planetary and Space Science*, 16(5), 615-646.

586 Gómez-Elvira, J., Armiens, C., Castañer, L., Domínguez, M., Genzer, M., Gómez,
587 F., ... & Martín-Torres, J. (2012). REMS: The environmental sensor suite for the Mars
588 Science Laboratory rover. *Space science reviews*, 170(1), 583-640.

589 Golombek, M. P. (1997). The mars pathfinder mission. *Journal of geophysical*
590 *research: Planets*, 102(E2), 3953-3965.

591 Guzewich, S., Newman, C., de la Torre Juarez, M., Wilson, R., Lemmon, M.,
592 Smith, M., ... Harri, A.(n.d.). the rem s science team and msl science team (2016).
593 Atmospheric tides in Gale Crater, Mars, *Icarus*, 268, 37–49.

Guzewich, S. D., de la Torre Juárez, M., Newman, C. E., Mason, E., Smith, M. D., Miller, N., ... Richardson, M. I. (2021). Gravity wave observations by the mars science laboratory rems pressure sensor and comparison with mesoscale atmospheric modeling with marswrf. *Journal of Geophysical Research: Planets*, 126(8), e2021JE006907.

Guzewich, S. D., Toigo, A. D., Richardson, M. I., Newman, C. E., Talaat, E. R., Waugh, D. W., & McConnochie, T. H. (2013). The impact of a realistic vertical dust distribution on the simulation of the Martian General Circulation. *Journal of Geophysical Research: Planets*, 118(5), 980-993.

Haberle, R. M., Joshi, M. M., Murphy, J. R., Barnes, J. R., Schofield, J. T., Wilson, G., ... & Schaeffer, J. (1999). General circulation model simulations of the Mars Pathfinder atmospheric structure investigation/meteorology data. *Journal of Geophysical Research: Planets*, 104(E4), 8957-8974.

Haberle, R., Gómez-Elvira, J., de la Torre Juárez, M., Harri, A.-M., Hollingsworth, J., Kahanpää, H., ... others(2014). Preliminary interpretation of the rems pressure data from the first 100 sols of the msl mission. *Journal of Geophysical Research: Planets*, 119(3), 440–453.

Haberle, R. M., Clancy, R. T., Forget, F., Smith, M. D., & Zurek, R. W. (2017). *The atmosphere and climate of mars*. Cambridge University Press.

Hess, S. L. , Henry, R. M. , Leovy, C. B. , Ryan, J. A. , Tillman, J. E. , & Chamberlain, T. E. , et al. (1976). Preliminary meteorological results on mars from the viking 1 lander. *Science*, 193(4255), 788-791.

616 Hess, S. L., Henry, R. M., Leovy, C. B., Ryan, J. A., Tillman, J. E., Chamberlain,
617 T. E., ... & Mitchell, J. L. (1976). Mars climatology from Viking 1 after 20 sols. *Science*,
618 194(4260), 78-81.

619 Hess, S., Henry, R., Leovy, C. B., Ryan, J., & Tillman, J. E. (1977). Meteorological
620 results from the surface of mars: Viking 1 and 2. *Journal of Geophysical Research*,
621 82(28), 4559–4574.

622 Hourdin, F., Van, P., Forget, F., & Talagrand, O. (1993). Meteorological variability
623 and the annual surface pressure cycle on mars. *Journal of the atmospheric sciences*,
624 50(21), 11.

625 Jackson, B. (2022). Vortices and dust devils as observed by the Mars
626 Environmental Dynamics Analyzer instruments on board the Mars 2020 Perseverance
627 rover. *The Planetary Science Journal*, 3(1), 20.

628 John Wilson, R., & Hamilton, K. (1996). Comprehensive model simulation of 284
629 thermal tides in the martian atmosphere. *Journal of Atmospheric Sciences*, 53(9), 1290–
630 1326.

631 Kleinböhl, A., John Wilson, R., Kass, D., Schofield, J. T., & McCleese, D. J. (2013).
632 The semidiurnal tide in the middle atmosphere of Mars. *Geophysical Research Letters*,
633 40(10), 1952-1959.

634 Lange, L., Forget, F., Banfield, D., Wolff, M., Spiga, A., Millour, E., ... others
635 (2022). Insight pressure data recalibration, and its application to the study of long-term
636 pressure changes on mars. *Journal of Geophysical Research: Planets*, 289
637 e2022JE007190.

638 Le Blancq, F. (2011). Diurnal pressure variation: the atmospheric tide. *Weather*,
 639 66(11), 306–307. Lomb, N. (1981). Least-squares frequency analysis of unequally
 640 spaced data. *Astrophys. Space*, 39.

641 Lindzen, R. S., & Chapman, S. (1969). Atmospheric tides. *Space science reviews*,
 642 10(1), 3-188.

643 Madeleine, J. B., Forget, F., Millour, E., Montabone, L., & Wolff, M. J. (2011).
 644 Revisiting the radiative impact of dust on Mars using the LMD Global Climate Model.
 645 *Journal of Geophysical Research: Planets*, 116(E11).

646 Madeleine, J. B., Forget, F., Millour, E., Navarro, T., & Spiga, A. (2012). The
 647 influence of radiatively active water ice clouds on the Martian climate. *Geophysical*
 648 *Research Letters*, 39(23).

649 Mart´inez, G., Newman, C., De Vicente-Retortillo, A., Fischer, E., Renno, N.,
 650 Richardson, M., ... others (2017). The modern near-surface martian climate: a review
 651 of in-situ meteorological data from viking to curiosity. *Space Science Reviews*, 212(1),
 652 295–338.

653 Montmessin, F., Forget, F., Rannou, P., Cabane, M., & Haberle, R. M. (2004).
 654 Origin and role of water ice clouds in the Martian water cycle as inferred from a general
 655 circulation model. *Journal of Geophysical Research: Planets*, 109(E10).

656 Montabone, L., Spiga, A., Kass, D. M., Kleinböhl, A., Forget, F., & Millour, E.
 657 (2020). Martian year 34 column dust climatology from Mars climate sounder
 658 observations: Reconstructed maps and model simulations. *Journal of Geophysical*
 659 *Research: Planets*, 125(8), e2019JE006111.

Navarro, T., Madeleine, J. B., Forget, F., Spiga, A., Millour, E., Montmessin, F., & Määttänen, A. (2014). Global climate modeling of the Martian water cycle with improved microphysics and radiatively active water ice clouds. *Journal of Geophysical Research: Planets*, 119(7), 1479-1495.

Rodriguez-Manfredi, J. A., De la Torre Juárez, M., Alonso, A., Apéstigue, V., Arruego, I., Atienza, T., ... & Zurita, S. (2021). The Mars Environmental Dynamics Analyzer, MEDA. A suite of environmental sensors for the Mars 2020 mission. *Space science reviews*, 217(3), 1-86.

Savijärvi, H., Määttänen, A., Kauhanen, J., & Harri, A. M. (2004). Mars Pathfinder: New data and new model simulations. *Quarterly Journal of the Royal Meteorological Society: A journal of the atmospheric sciences, applied meteorology and physical oceanography*, 130(597), 669-683.

She, C. Y., Krueger, D. A., Yuan, T., & Oberheide, J. (2016). On the polarization relations of diurnal and semidiurnal tide in the mesopause region. *Journal of Atmospheric and Solar-Terrestrial Physics*, 142, 60-71.

Scargle, J., & D. (1982). Studies in astronomical time series analysis. ii – statistical aspects of spectral analysis of unevenly spaced data. *ApJ*, 263(2), 835-835.

Spiga, A., Banfield, D., Teanby, N. A., Forget, F., Lucas, A., Kenda, B., ... others (2018). Atmospheric science with insight. *Space Science Reviews*, 214(7), 1–64.

Spiga, A., Murdoch, N., Lorenz, R., Forget, F., Newman, C., Rodriguez, S., ...others (2021). A study of daytime convective vortices and turbulence in the martian planetary boundary layer based on half-a-year of insight atmospheric measurements and large-

eddy simulations. *Journal of Geophysical Research: Planets*, 126(1), e2020JE006511.

Tillman, J. E. (1988). Mars global atmospheric oscillations: Annually synchronized, transient normal-mode oscillations and the triggering of global dust storms. *Journal of Geophysical Research: Atmospheres*, 93(D8), 9433–9451.

Viu'dez-Moreiras, D., Newman, C., Forget, F., Lemmon, M., Banfield, D., Spiga, A., ... others (2020). Effects of a large dust storm in the near-surface atmosphere as measured by insight in elysium planitia, mars. comparison with contemporaneous measurements by mars science laboratory. *Journal of Geophysical Research: Planets*, 125(9), e2020JE006493.

Wilson, R. J., Banfield, D., Conrath, B. J., & Smith, M. D. (2002). Traveling waves in the northern hemisphere of mars. *Geophysical research letters*, 29(14), 29–1.

Wilson, R. J., & Guzewich, S. D. (2014). Influence of water ice clouds on nighttime tropical temperature structure as seen by the Mars Climate Sounder. *Geophysical Research Letters*, 41(10), 3375-3381.

Wu, Z., Li, T., & Dou, X. (2015). Seasonal variation of martian middle atmosphere 320 tides observed by the mars climate sounder. *The Journal of Geophysical Research Planets*, 120(12), n/a-n/a.

Wu, Z., Li, T., & Dou, X. (2017). What causes seasonal variation of migrating 323 diurnal tide observed by the mars climate sounder? *Journal of Geophysical Research: Planets*, 122(6).

Wu, Z., Li, T., Zhang, X., Li, J., & Cui, J. (2020). Dust tides and rapid meridional motions in the Martian atmosphere during major dust storms. *Nature*

704 communications, 11(1), 1-10.

705 Wu, Z., T. Li, N. G. Heavens, C. E. Newman, M. I. Richardson, C. Yang, J. Li, and
706 J. Cui (2022), Earth-like thermal and dynamical coupling processes in the Martian
707 climate system, Earth-Science Reviews, 229, 104023,
708 doi:<https://doi.org/10.1016/j.earscirev.2022.104023>.

709 Zurek, R. W. (1976). Diurnal tide in the Martian atmosphere. Journal of the
710 Atmospheric Sciences, 33(2), 321-337.

711 Zurek, R. W., & Leovy, C. B. (1981). Thermal tides in the dusty Martian
712 atmosphere: A verification of theory. Science, 213(4506), 437-439.

713

Observed dawn and twilight surface pressure fluctuation in the Martian tropics and possible relationships with the atmospheric tides

Chengyun Yang^{1,2,3#}, Cong Sun^{2#}, Zhaopeng Wu^{3,4}, and Tao Li^{1,2,3*}

¹Deep Space Exploration Laboratory / School of Earth and Space Sciences, University of Science and Technology of China, Hefei, Anhui, China

² CAS Key Laboratory of Geospace Environment, School of Earth and Space Sciences, University of Science and Technology of China, Hefei, Anhui, China

³ CAS Center for Excellence in Comparative Planetology, University of Science and Technology of China, Hefei, Anhui, China

⁴ Planetary Environmental and Astrobiological Research Laboratory, School of Atmospheric Sciences, Sun Yat-sen University, Zhuhai 519082, China

Correspondence to: Tao Li (litao@ustc.edu.cn)

The authors contributed equally to this work

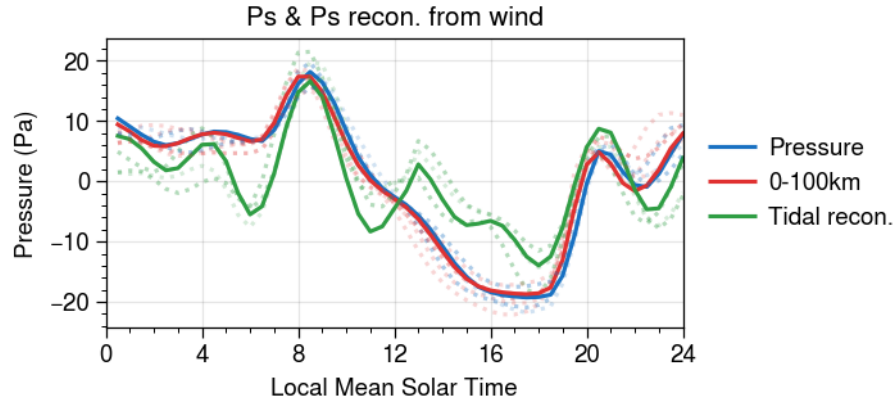


Figure S1. Same as Figure 6a, but in Insight sols ranging from 75-140. The blue line is the demeaned surface pressure in 10 sols mean, the solid blue line is in the sol 125-135, which is same as Figure 2 in the paper, the dotted blue line is the demeaned surface pressure in other sols; the red lines are same as the blue lines but show the surface pressure reconstruction from 0-100 km horizontal winds; the green line are same as the red lines but show the surface pressure reconstructed from the tidal wind, whose components are similar with the paper. As we can see, both the reconstruction from the original winds and the tidal winds agree with the DTPs in the present time and relative amplitude in the sols near equinox.